Stoichiometry Controlled Bipolar Conductivity in Nanocrystalline $Ni_xCd_{1-x}O_{1+\delta}$ Thin Films

Chao Ping Liu,[1,4] Kingsley O. Egbo,[1] Chun Yuen Ho,[1] Juan Antonio Zapien,[2] W. Walukiewicz,[3] and Kin Man Yu[1,2,*]

[1]*Department of Physics, City University of Hong Kong, 83 Tat Chee Ave., Kowloon, Hong Kong*
[2]*Department of Materials Science and Engineering, City University of Hong Kong, 83 Tat Chee Ave., Kowloon, Hong Kong*
[3]*Materials Sciences Division, Lawrence Berkeley National Laboratory, Berkeley, California 94720, USA*
[4]*Department of Physics, College of Science, Shantou University, Shantou, Guangdong 515063, China*

Wide-gap oxides exhibiting both *n*- and *p*-type bipolar conductivity are extremely desirable for the development of next generation transparent optoelectronics. While most metal oxides show a propensity for *n*-type conductivity, nickel oxide (NiO) is one of the few that exhibits *p*-type conductivity without intentional doping. We synthesize nanocrystalline-$Ni_xCd_{1-x}O_{1+\delta}$-alloy thin films over the entire composition range with variable crystal stoichiometry using RT radio-frequency magnetron sputtering. Optical and electronic properties of the films are investigated with a variety of experimental techniques, including spectroscopic ellipsometry, the Seebeck effect, and the variable-temperature Hall effect as well as x-ray photoelectron spectroscopy. We find that the conduction type of $Ni_xCd_{1-x}O_{1+\delta}$-alloy thin films depends on the alloy composition and oxygen stoichiometry. Stoichiometric $Ni_xCd_{1-x}O$ alloys are *n* type in the composition range of $0 \leq x \leq 0.52$ and insulating for higher *x*. On the other hand, O-rich alloys are *p*-type conducting for $x \geq 0.38$. This demonstrates that in the alloy composition range of $0.38 < x < 0.52$, *n*-type and *p*-type $Ni_xCd_{1-x}O$ alloys can be synthesized by controlling the oxygen stoichiometry. The unusual electrical and optical properties of $Ni_xCd_{1-x}O_{1+\delta}$-alloy thin films can be explained by the modifications of the electronic band structure due to anticrossing interactions between localized Ni *d* levels and extended valence and conduction band states of the alloy. The results offer an interesting opportunity for using $Ni_xCd_{1-x}O_{1+\delta}$ alloys for transparent devices that require bipolar conductivity.

I. INTRODUCTION

Wide-gap transparent metal oxides have been extensively studied because of their applications as transparent contacts for solar power conversion and potential applications as active materials in transparent electronics [1–3]. Currently, the development of transparent oxide electronics is hampered by the lack of wide-gap oxides with bipolar conductivity. In most metal oxides, the valence band edge (VBE) states are derived from O *2p* orbitals and are located very low on the absolute scale, making efficient *p*-type doping of these materials very challenging [4,5]. On the other hand, because of the low location of the conduction-band (CB) edge (CBE), many metal oxides (e.g., ZnO, In_2O_3, CdO, or SnO_2) show strong proclivity for *n*-type conductivity. These oxides can be heavily doped with donors and are widely used as transparent conductors in photovoltaic and optoelectronic devices [6–9]. Recently, considerable efforts have been devoted

to the design and development of different *p*-type transparent oxides based on the idea of modifying the valence band (VB) dispersion through chemical alloying [10–13]. Kawazoe *et al.* reported a pioneering study of $CuAlO_2$-based *p*-type oxides [10] and this work has generated an intense interest in the Cu^+-based delafossite oxides with the general chemical formula $CuMO_2$ ($M = $ B, Al, Cr, Ga, Sc, In, or Y) [14]. However, deposition of these Cu^+-based delafossites typically requires a high substrate temperature (approximately 500 °C) grown on a single-crystalline sapphire substrate [10,11], limiting their applications for plastic optoelectronics. There are several material requirements for the development of transparent bipolar devices, including, *p*- and *n*-type materials with similar lattice parameters, electrical mobility, and conductivity, as well as matching thermal-expansion coefficients and fabrication temperatures [15]. Hence, a realization of bipolar doping in wide-gap oxides is extremely challenging, and thus far, limited bipolar conductivity has been reported for only three metal oxides: $CuInO_2$, SnO, and ZrOS [16–18].
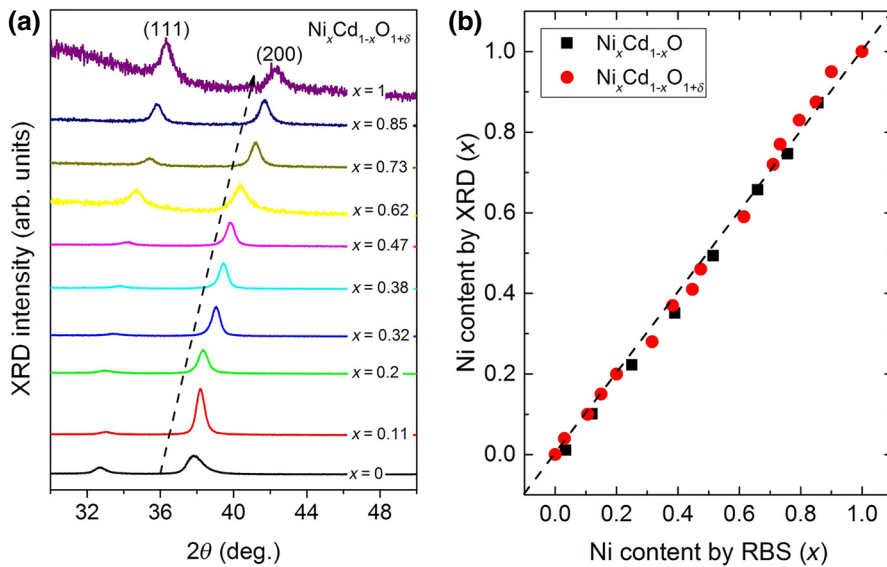
*kinmanyu@cityu.edu.hk

FIG. 1. (a) GIXRD spectra of as-sputtered $Ni_xCd_{1-x}O_{1+\delta}$-alloy films with different Ni content x, and the dashed line indicates the shift of (200) peak position with increasing x; (b) the calculated x from XRD spectra using Vegard's law as a function of Ni content x from RBS measurements, with the black squares and red circles denoting the alloy samples sputtered in pure Ar and 1.4% O_2, respectively.

One of the very few known wide-gap binary oxides exhibiting *p*-type conductivity is nickel oxide (NiO) [19,20]. Stoichiometric NiO is a Mott-Hubbard insulator, while *p*-type conductivity can be realized by extrinsic doping (e.g., with Li or Cu) or by native defects such as nickel vacancies and/or interstitial oxygen [21–25]. Typical conductivity in the range of 1 to 10 S/cm can be obtained in NiO with transparencies of approximately 40%–60% in the visible range [19]. The origin of the *p*-type conductivity can be attributed to an unusually high location of the VBE at approximately 4.8 eV below the vacuum level [26,27]. This, combined with the large band gap of 3.7 eV, makes NiO a very attractive material for transparent-hole transport-electron blocking layers in optoelectronic devices [28–30].

Among *n*-type oxides, cadmium oxide (CdO) plays a special role because of its very high conductivity associated with very high electron concentration of $>10^{21}/cm^3$ and mobility larger than 100 cm^2/V s. The heavily *n*-type doped CdO has received renewed interest in recent years as a transparent conductor for full-spectrum-photovoltaics applications [31–33]. Both CdO and NiO have the same rock salt crystal structure. However, the large difference between those two materials is the location of the CBE and the VBE with the CB minimum (CBM) of CdO located about 1 eV below the VB maximum (VBM) of NiO [34–37]. Hence, CdO and NiO have an extreme type III band offset and their alloys offer a range of materials with a wide tunability not only of the band gap (from 2.2 to 3.7 eV), but also of the CB and the VB offsets (4.5 and 3 eV, respectively). An important feature of the NiO-CdO alloy system is that it offers a unique opportunity for the development of wide-gap oxide materials exhibiting bipolar conductivity.

Systematic studies on the electronic band structure as well as the optoelectrical properties of $Ni_xCd_{1-x}O$-alloy thin films synthesized by magnetron sputtering at an elevated substrate temperature (270 °C) in pure Ar gas over the entire composition range have been reported [36,38]. It was found that the electron mobility and the electron concentration of $Ni_xCd_{1-x}O$-alloy thin films decrease with increasing x and the alloy films become insulating for $x > 0.44$ [36]. In this paper, we report on the synthesis of transparent $Ni_xCd_{1-x}O_{1+\delta}$-alloy thin films over the entire composition range at RT, with δ denoting the deviation in O stoichiometry. We find that alloy films are nanocrystalline and their conduction type (*n* or *p*) depends on the Ni content and O stoichiometry. By controlling the deposition conditions, we demonstrate that $Ni_xCd_{1-x}O_{1+\delta}$ alloys can exhibit bipolar conductivity within a composition range x of approximately 0.38–0.52.

II. EXPERIMENT

$Ni_xCd_{1-x}O_{1+\delta}$-alloy films are grown on glass substrates using a multigun radio-frequency magnetron sputtering system with separate NiO and CdO targets without intentional substrate heating. The oxygen flow ratio $f(O_2)/[f(Ar) + f(O_2)]$ in the sputtering gas is fixed to be 0% (pure Ar) or 1.4%, unless stated otherwise. Alloy composition is controlled by varying the sputtering power of the individual targets. The composition and thickness of alloy films are determined by Rutherford backscattering spectrometry (RBS) using a 3.04-MeV He^{2+} beam. The film structure is analyzed by grazing incidence x-ray diffraction (GIXRD) with a grazing incidence angle of 1°. Optical properties of alloy films are studied by spectroscopic ellipsometry (SE) in the spectral range of

0.74–6.45 eV. Electrical properties are investigated by variable-temperature (300–450 K) Hall-effect measurements in the van der Pauw configuration using an Ecopia HMS-5300 system, while the RT Seebeck measurements are conducted to verify the p- or n-type conductivity. High-resolution x-ray photoelectron spectroscopy (XPS) measurements are performed using a monochromatic Al $K\alpha$ x-ray source ($h\nu = 1.487$ keV). Photoelectrons are collected and analyzed with a concentric hemispherical analyzer.

III. RESULTS AND DISCUSSTION

A. Crystal structure

The RT-sputtered alloy films have a rock salt crystal structure in the whole composition range with a film thickness in the range of 50–110 nm. In the following, we will use $Ni_xCd_{1-x}O$ and $Ni_xCd_{1-x}O_{1+\delta}$ to denote alloy films sputtered in pure Ar ($O_2\% = 0\%$) and $Ar + O_2$ ($O_2\% = 1.4\%$), respectively. Although their exact stoichiometry cannot be measured, hereafter these films will be referred to as stoichiometric ($Ni_xCd_{1-x}O$) and nonstoichiometric ($Ni_xCd_{1-x}O_{1+\delta}$) films. In our RBS measurements, we utilize the $^{16}O(\alpha,\alpha)^{16}O$ resonant scattering condition at 3.04 MeV so that the O sensitivity is enhanced to within 2%. Our measurements verify that films sputtered with additional O_2 contain up to 10% more O (i.e., $\delta \sim 0.1$) as compared to those sputtered in Ar only. However, the exact O composition is still difficult to quantify because of uncertainties in the resonant scattering cross section of O. Figure 1(a) shows GIXRD spectra of selected as grown $Ni_xCd_{1-x}O_{1+\delta}$-alloy films with different Ni content (x). Note that all the films deposited at RT are crystalline with

the rock salt (111) ($2\theta \sim 33$–$36°$) and (200) ($2\theta \sim 38$–$42°$) diffraction peaks shifting to higher angles corresponding to smaller interplanar distances as x increases. Since the lattice parameters of CdO (a_{CdO}) and NiO (a_{NiO}) are 4.72 and 4.19 Å, respectively, this is consistent with the formation of random alloys with decreasing lattice parameter as x increases. The Ni content x in the alloy films has been calculated from the lattice parameter $a(x)$ derived from the diffraction peaks using Vegard's law $a(x) = xa_{NiO} + (1-x)a_{CdO}$. Figure 1(b) shows the Ni content obtained from the diffraction patterns in comparison to x measured by RBS. While RBS measures the total Ni atoms in the films regardless of their specific sites, x obtained from XRD reveals Ni atoms substituting Cd in the alloy. The excellent agreement of Ni contents in all alloy films sputtered with and without additional O_2 shown in Fig. 1(b) suggests all Ni atoms are incorporated in the alloy with no significant secondary phase present. The grain size of $Ni_xCd_{1-x}O_{1+\delta}$-alloy films calculated from the Scherrer equation ranges from 3 to 22 nm. Interestingly, the RT-sputtered Ni-rich $Ni_xCd_{1-x}O$-alloy film ($x > 0.5$) exhibits higher crystallinity than that of $Ni_xCd_{1-x}O_{1+\delta}$-alloy films with similar Ni content.

B. Optical properties

The optical properties of these RT-sputtered CdO-NiO-alloy films are studied by SE. In order to evaluate the effect of additional oxygen on the optical properties, we compare the transmission spectra [Fig. 2(a)] and the absorption coefficient [Fig. 2(b)] for alloy films with similar Ni content sputtered in pure Ar and in 1.4% O_2. Figure 2(a) shows the optical transmission spectra of
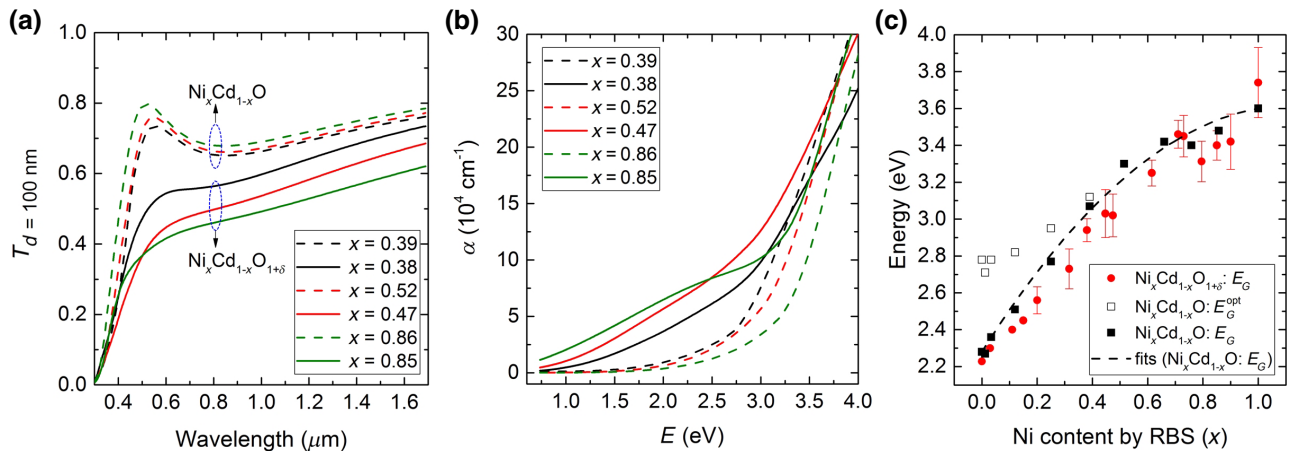

FIG. 2. (a) A comparison of transmission spectra of typical $Ni_xCd_{1-x}O$- (i.e., sputtered in pure Ar, denoted as dotted lines) and $Ni_xCd_{1-x}O_{1+\delta}$-alloy films (i.e., sputtered in 1.4% O_2, denoted as solid lines) with similar Ni contents calculated for 100-nm-thick films from SE measurements; (b) the corresponding absorption coefficient for these films derived from SE analysis; (c) intrinsic band gap (E_G) of $Ni_xCd_{1-x}O$- (solid black squares) and $Ni_xCd_{1-x}O_{1+\delta}$- (solid red circles) alloy thin films as a function of x; the open black squares are the optical absorption edges (E_G^{Opt}). A quadratic fit of the $Ni_xCd_{1-x}O$ intrinsic band gaps using a bowing parameter $b = -1.05$ is shown as the black dashed line.

100-nm-thick films for typical alloy films on glass substrates. As seen, $Ni_xCd_{1-x}O_{1+\delta}$-alloy films exhibit lower transparency (40%–70%) than stoichiometric $Ni_xCd_{1-x}O$ films (70% to 80%) with similar Ni contents. With increasing x, the difference in transparency between $Ni_xCd_{1-x}O$- and $Ni_xCd_{1-x}O_{1+\delta}$-alloy films increases. We also note that the NiO thin films sputtered with higher O_2 contents (>20% of O_2) exhibit even lower transparency (e.g., <40%) [19]. The absorption coefficients (α) of typical alloy films are shown in Fig. 2(b). Note that $Ni_xCd_{1-x}O_{1+\delta}$-alloy films exhibit substantial subgap absorption with $\alpha \sim 3-5 \times 10^4$ cm^{-1} at 2 eV. This is similar to the subgap absorption previously observed in nonstoichiometric O-rich NiO films [39,40]. For the O-rich NiO, the nonstoichiometry gives rise to native acceptor defects, namely Ni vacancies V_{Ni} and O interstitials O_i. The high subband-gap absorption has been attributed to these native defects, in particular V_{Ni}-induced p–d charge transfer transitions and/or to the d–d crystal-field transitions. The magnitude of the subgap absorption qualitatively describes the degree of the NiO nonstoichiometry, which, in turn, affects the p-type conductivity of the film. For the NiO-rich $Ni_xCd_{1-x}O_{1+\delta}$ alloys, we believe that the origin of the subgap absorption is similar to that of NiO.

The optical absorption edges (E_G^{Opt}) of $Ni_xCd_{1-x}O$-alloy films are estimated by extrapolating the α^2 vs photon energy plots to the energy intercept. With increasing x, the E_G^{Opt} of RT-sputtered $Ni_xCd_{1-x}O$-alloy film shows a monotonous increase from 2.78 eV ($x=0$) to 3.6 eV ($x=1$). The intrinsic band gap (E_G) can be obtained by taking into account the Burstein-Moss shift and the band-gap renormalization [41,42]. The Burstein-Moss effect will increase the optical band gap (ΔE_G^{BM}), while the band-gap-renormalization effect due to the electron-electron interaction and electron-ion interaction would narrow the optical band gap (ΔE^{BGN}), i.e., $E_G^{opt} = E_G + \Delta E_G^{BM} - \Delta E^{BGN}$. The parameter values used for calculating the band-gap renormalization are adopted from work by Zhu *et al.* [43]. It is worth noting that both the Burstein-Moss shift and the band-gap renormalization become negligible when the carrier density (N) is lower than 10^{19} cm^{-3}. As shown in Fig. 2(c) for $Ni_xCd_{1-x}O$ with $x < 0.4$, since $N > 10^{19}$/cm^3 (Fig. 3), E_G^{Opt} (open black squares) are significantly higher than E_G (solid black squares). A bowing parameter b is commonly used to describe the deviation of the band gap of a semiconductor alloy A_xB_{1-x} from Vegard's law, $E_G(x) = xE_A + (1-x)E_B - bx(1-x)$. A quadratic fit of the $Ni_xCd_{1-x}O$ intrinsic band gaps using a bowing parameter $b = -1.05$ is shown as the black dashed line in Fig. 2(c). It is found that E_G of these RT-deposited $Ni_xCd_{1-x}O$-alloy films increases from 2.28 to 3.6 eV as x increases from 0 to 1, with a positive band-gap bowing ($b = -1.05$). This is similar to the positive bowing with $b = -1.26$ eV previously reported by Francis *et al.* for stoichiometric
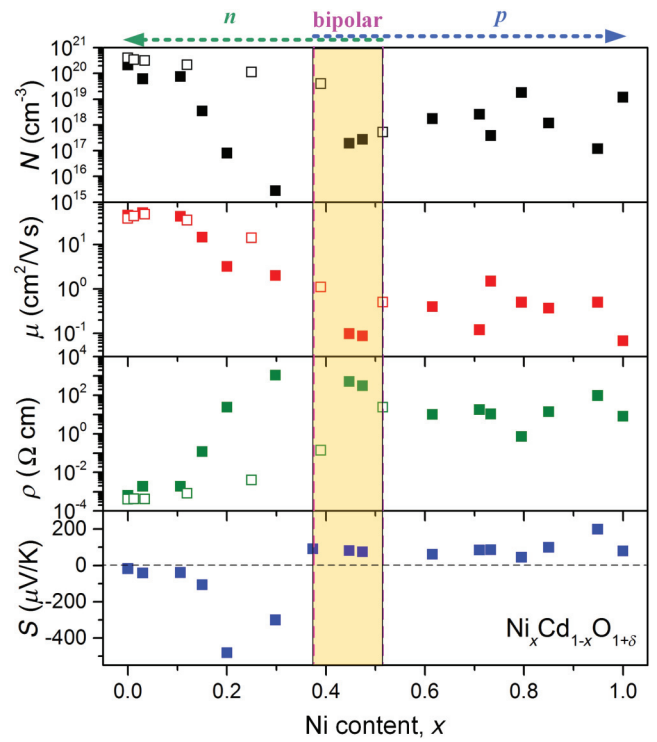

FIG. 3. RT electrical properties of as-grown $Ni_xCd_{1-x}O_{1+\delta}$-alloy films (denoted by solid squares) in the entire composition range. From top to bottom panels, they are carrier density (N), Hall mobility (μ), resistivity (ρ), and Seebeck coefficient (S), respectively. The electrical properties of RT-deposited $Ni_xCd_{1-x}O$-alloy films (denoted by open squares) are also shown for comparison.

$Ni_xCd_{1-x}O$-alloy films sputter deposited at 270 °C [36], but is in contrast to the negative bowings commonly observed for most semiconductor alloys. The anomalous positive band-gap bowing for $Ni_xCd_{1-x}O$ alloys has been explained previously by a band anticrossing (BAC) interaction between localized $3d$ states of Ni and the extended states of the $Ni_xCd_{1-x}O$-alloy host [38]. For comparison, the E_G of $Ni_xCd_{1-x}O_{1+\delta}$-alloy films are also shown (solid red circles) in Fig. 2(c). Given the high subgap absorption for $Ni_xCd_{1-x}O_{1+\delta}$-alloy films with $x > 0.2$, their E_G^{opt} are obtained by extrapolating the α^2 to zero with appropriate background subtraction. Accordingly, error bars due to the high background subgap absorption of $Ni_xCd_{1-x}O_{1+\delta}$ with $x > 0.2$ are also included. Note that for both $Ni_xCd_{1-x}O$ and $Ni_xCd_{1-x}O_{1+\delta}$ alloys with similar x, their band gaps are also similar.

C. Electrical transport mechanism and electronic band structure

The electrical properties of both $Ni_xCd_{1-x}O$- (open squares) and $Ni_xCd_{1-x}O_{1+\delta}$- (closed squares) alloy films with different x are presented in Fig. 3. When sputtered in pure Ar, $Ni_xCd_{1-x}O$ samples are n-type conducting

for $x < 0.5$, with N and μ decreasing from 4×10^{20} to $<10^{18}$/cm^3 and 50 to <1 cm^2/V s, respectively, as x increases from 0 to 0.5. It is worth noting that the RT-sputtered Ni$_x$Cd$_{1-x}$O samples shown in Fig. 3 have very close electron concentrations to those sputtered at a high substrate temperature (approximately 270 °C) [36]. Similarly, as will be discussed later, the decrease in electron concentration of RT-deposited Ni$_x$Cd$_{1-x}$O with increasing Ni content can be attributed to the upward shift of the CBM, resulting in reduced propensity of material for n-type doping [32,38].

As seen in Fig. 3, the electron concentration in CdO-rich Ni$_x$Cd$_{1-x}$O$_{1+\delta}$ is much lower and drops much faster from 10^{20} to $<10^{16}$/cm^3 as x increases from 0 to 0.3 than in Ni$_x$Cd$_{1-x}$O. This suggests that adding O$_2$ makes the films O-rich or group-II-element (Cd or Ni) deficient resulting in reduced concentration of O vacancy donors and increased concentration of group-II-vacancy acceptors. Carrier compensation due to acceptor defects in O-rich alloys also results in a lower mobility compared to stoichiometric Ni$_x$Cd$_{1-x}$O films with similar composition. We note that for Cd-rich Ni$_x$Cd$_{1-x}$O$_{1+\delta}$ alloys ($0 < x < 0.4$), the electron concentration can be controlled within the range of

10^{20}–10^{17}/cm^3 by adjusting the alloy composition and the amount of O$_2$ in the sputtering gas. In alloy films with $x > 0.3$, the mobility falls below 2 cm^2/V s and can be as low as 0.1 cm^2/V s, consequently the conductivity type determined from the Hall effect using a typical magnetic field of 0.5 T becomes ambiguous. In order to reliably determine the conductivity type, we also perform thermopower measurements on these samples. The Seebeck coefficients (S) for Ni$_x$Cd$_{1-x}$O$_{1+\delta}$ samples are also plotted in the lower panel of Fig. 3. Ni$_x$Cd$_{1-x}$O$_{1+\delta}$ films with $x \leq 0.3$ exhibit negative S, confirming that alloys in this composition range are indeed n type.

Unlike Ni$_x$Cd$_{1-x}$O, which is insulating for $x > 0.52$, Ni$_x$Cd$_{1-x}$O$_{1+\delta}$ films exhibit p-type conductivity for Ni content $x \geq 0.38$. This is evidenced by the positive S for these samples as shown in Fig. 3. As mentioned earlier, due to the low hole mobility in Ni$_x$Cd$_{1-x}$O$_{1+\delta}$, the hole concentration and μ obtained from RT Hall-effect measurements are unreliable. However, using variable-temperature Hall-effect measurements (shown in Fig. 4), we have found that the hole mobility increases with temperature and becomes higher than 1 cm^2/V s for $T \geq 400$ K. At the same time, the hole concentration does not significantly change with

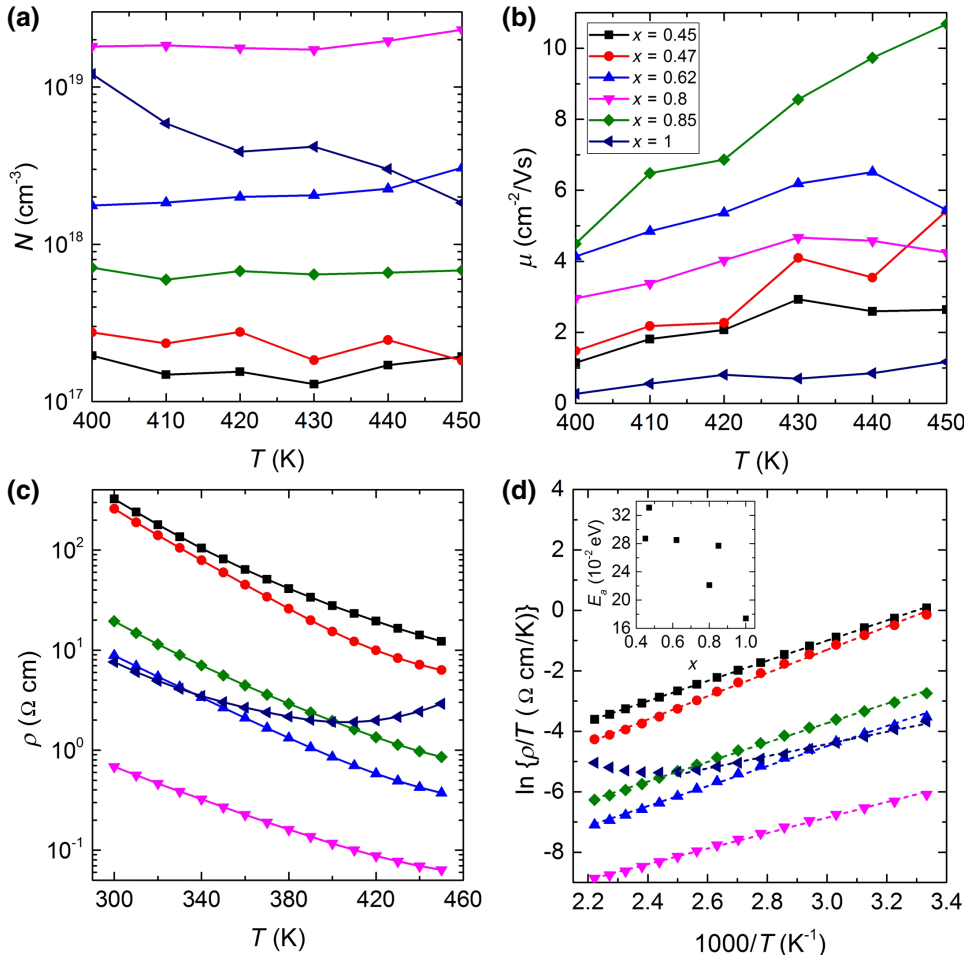FIG. 4. Temperature-dependent electrical properties from Hall effect measurement for p-type Ni$_x$Cd$_{1-x}$O$_{1+\delta}$ films in the temperature range of 300–450 K, (a) the hole concentration N, (b) the hole mobility μ, (c) the resistivity ρ as a function of measurement temperature T, and (d) plots of $\ln(\rho/T) \sim 1/T$ as well as the corresponding fits (dotted lines), with the inset showing the corresponding E_a of Ni$_x$Cd$_{1-x}$O$_{1+\delta}$ films vs Ni content x.

temperature. Hence, we can reasonably assume the hole concentration $N(\text{RT}) = N(400\ \text{K})$ and estimate the RT hole mobility from the RT resistivity. The estimated RT hole mobility of *p*-type $Ni_xCd_{1-x}O_{1+\delta}$ films ranges from 0.07 cm²/V s for $x = 1$ to 1.5 cm²/V s for $x = 0.73$, as shown in Fig. 3. Note that the estimated RT hole mobility for the $NiO_{1+\delta}$ film (i.e., approximately 0.07 cm²/V s) is similar to those previously reported for ceramic NiO samples [44,45].

The low hole mobility of $Ni_xCd_{1-x}O_{1+\delta}$ may raise concern about their practical applications in optoelectronics, since high carrier mobility is generally preferred for devices. For example, carrier mobility directly affects the maximum drain current and the operating frequency for thin-film transistors, and high mobility (on the order of 10 cm²/V s) is typically required for driving displays with higher resolution, faster frame rate, and larger panel size [46]. While low carrier mobility limits the applications for devices, it may not be a determining factor for certain optoelectronic applications. For instance, low-mobility NiO ($\mu < 0.1$ cm²/V s) has been used to fabricate NiO/ZnO hetero *p-n* junctions for transparent oxide-based UV-sensitive solar cells [47] or adopted as the efficient hole transporting layer for high-performance perovskite solar cells [48,49]. Note that for most transparent oxide devices, the film thickness is rather thin (on the order of 10–100 nm) and hence the low carrier mobility is not detrimental to the device. Furthermore, from Fig. 3, we note that *n*-type $Ni_xCd_{1-x}O$ (particularly with $x < 0.4$) has a higher mobility of >1 cm²/V s and can be used as the thicker active layer for a "quasi-homo" *p-n* junction device where the *p* layer is slightly more Ni rich (e.g., $x \sim 0.45$). Hence, we believe that the *p*-type (including the bipolar region) $Ni_xCd_{1-x}O_{1+\delta}$ alloys would have great potential applications for emerging oxide-based bipolar optoelectronics [50]

The resistivity of *p*-type $Ni_xCd_{1-x}O_{1+\delta}$ films can be further lowered by increasing the O_2 partial pressure in the sputtering gas. For instance, by increasing the O_2 from 1.4% to 4%, the resistivity of $Ni_{0.62}Cd_{0.38}O_{1+\delta}$-alloy film drops by almost an order of magnitude from 10.2 to 1.4 Ω cm. Hence, both *n*-type and *p*-type $Ni_xCd_{1-x}O_{1+\delta-}$alloy films can be obtained by controlling the O stoichiometry in the alloy composition range $0.38 < x < 0.52$. Thus, it should be possible to construct *p-n* homojunctions between *n* $Ni_xCd_{1-x}O$ and *p* $Ni_xCd_{1-x}O_{1+\delta}$ in this composition range.

Variable-temperature (from 300–450 K) Hall measurements (N, μ, and ρ) for the *p*-type samples ($0.45 \leq x \leq 1$) are shown in Fig. 4. Except for $NiO_{1+\delta}$, the hole concentration for the alloy films is rather insensitive to temperature. N for $NiO_{1+\delta}$ drops drastically from 1.2×10^{19} cm⁻³ at $T = 400$ K to 1.8×10^{18} cm⁻³ at $T = 450$ K, but does not go back to its original value as the temperature decreases. This can be attributed to the thermal instability of O-induced

nickel vacancies or the O interstitials in the $NiO_{1+\delta}$ film [19]. The hole concentration at 400 K for these *p*-type $Ni_xCd_{1-x}O_{1+\delta}$-alloy films ranges from 1.9×10^{17} cm⁻³ ($x = 0.45$) to 1.8×10^{19} cm⁻³ ($x = 0.8$) and they vary only slightly with temperature, suggesting that the as sputtered *p*-type $Ni_xCd_{1-x}O_{1+\delta}$-alloy films are thermally stable up to 450 K. In contrast, the hole mobility of these *p*-type $Ni_xCd_{1-x}O_{1+\delta}$-alloy films increases with temperature [see Fig. 4(b)], for example, the mobility of the alloy film with $x \sim 0.85$ increases from approximately 4.5 to 10.6 cm²/V s, while its hole concentration only shows a slight variation from approximately 7.1×10^{17} to 6.8×10^{17} cm⁻³ as the temperature increases from 400 to 450 K. This suggests that the conduction process in these *p*-type $Ni_xCd_{1-x}O_{1+\delta}$-alloy films is mainly due to the thermal excitation of the mobility [(i.e., small polaron hopping (SPH)], similar to the conduction process found in nonstoichiometric $NiO_{1+\delta}$ [21]. Figure 4(c) shows the resistivity ρ in the range of 300–450 K. As expected, the ρ of these *p*-type $Ni_xCd_{1-x}O_{1+\delta}$-alloy films decreases with increasing T, with the exception of the $NiO_{1+\delta}$ film at relatively high T due to its thermal instability. According to the SPH model, the temperature-dependent resistivity can be expressed by $\rho/T = \rho_0 \exp(E_a/kT)$, where k is the Boltzmann constant and E_a is the activation energy [51–53]. Figure 4(d) further plots the fit of temperature-dependent resistivity data based on the SPH model [i.e., $\ln(\rho/T) \sim 1/T$]. It can be seen that the data fit well with the SPH in the range of 300–450 K. It is worth noting that the fit for the $NiO_{1+\delta}$ film is limited to the temperature range of 300–400 K in
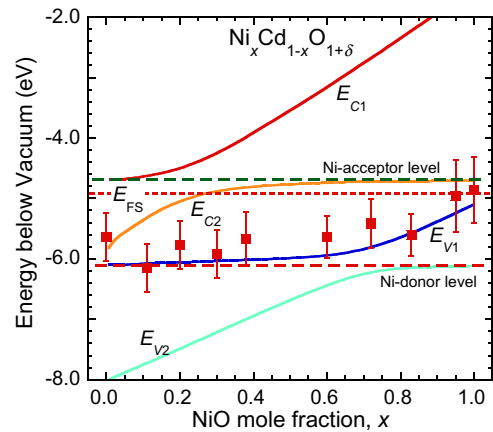

FIG. 5. Calculated subband energies for $Ni_xCd_{1-x}O_{1+\delta}$ using the BAC model [38]. Band-edge energies, i.e., VBM values obtained by fitting the XPS valence-band spectra (square symbols) are also plotted. Here, E_{C1} and E_{C2} correspond to conduction subbands formed by the anticrossing interaction of the extended host CB and the localized Ni *d* acceptor states, while E_{V1} and E_{V2} are the valence subbands formed by the anticrossing interaction of the extended host valence band and the localized Ni *d* donor states.

order to reduce the effect of thermal instability at relatively higher temperatures. The E_a extracted from the slopes of the fits varies from 0.174 eV ($x = 1$) to 0.331 eV ($x = 0.47$), as depicted in the inset of Fig. 4(d). The E_a for the $NiO_{1+\delta}$ film is comparable to values reported previously by others (e.g., 0.17 eV for $NiO_{1.07}$, 0.224 eV for $Li_{0.006}Ni_{0.994}O$) [54,55].

The electrical and optical properties of the studied $Ni_xCd_{1-x}O$- and $Ni_xCd_{1-x}O_{1+\delta}$-alloy films can be qualitatively understood in terms of the previously developed electronic band structure that considers BAC interaction between acceptor and donor levels associated with a partially filled Ni d-shell and extended band states of the host matrix [38]. As seen in Fig. 5, the d-acceptor level is located well above the CBM of CdO-rich alloys and close to the VBM in Ni-rich alloys, whereas the d-donor level lies close to the CBM in CdO-rich alloys and well below the VBM in NiO-rich alloys. An anticrossing interaction between these localized states and the extended states of the host matrix results in the formation of two valence (E_{V1}, E_{V2}) and two conduction (E_{C1} and E_{C2}) subbands. The character of the states (extended or localized) depends on the location of a given band relative to the highly localized d-levels. Thus, in the CdO-rich and NiO-rich compositions, the highest valence subband E_{V1} and lowest conduction subband E_{C2}, respectively, lie in close proximity to the d levels and are narrow and highly localized. Consequently, they do not contribute to optical absorptions.

The composition dependence of the doping behavior and the electrical properties of the $Ni_xCd_{1-x}O_{1+\delta}$ alloys are determined by the location of the CBM and VBM relative to the Fermi stabilization energy E_{FS} located at 4.9 eV below the vacuum level [36,56]. In CdO-rich stoichiometric $Ni_xCd_{1-x}O$, the E_{C2} is located well below E_{FS} and the n-type electrical conductivity is determined by the low formation energy of donors. As seen in Fig. 5, E_{C2} shifts up with increasing Ni content resulting in larger donor defect-formation energy and lower electron concentration. The upward shift of the E_{C2} explains a large reduction of the electron concentration shown in Fig. 3 and reported in Ref [38]. In addition, with increasing NiO content, the E_{C2} subband evolves from a band of fully extended states in the CdO-rich alloy to a narrow strongly localized band in the intermediate composition range. This explains the rapid reduction in the electron mobility with increasing NiO content shown in Fig. 3. The reduction of the electron concentration and electron mobility produces a material with immeasurable resistivity for $x > 0.52$.

In order to understand the difference between the properties of the stoichiometric and O-rich $Ni_xCd_{1-x}O$ alloys, we note that increasing the O chemical potential reduces the formation energy of acceptor-like cation (Cd or Ni) vacancies. Since, as has been discussed above, increasing the NiO content in CdO-rich $Ni_xCd_{1-x}O_{1+\delta}$ alloys increases the formation energy and decreases the concentration of donor defects, therefore, the excess O-induced acceptor defects efficiently compensate these donors leading to a
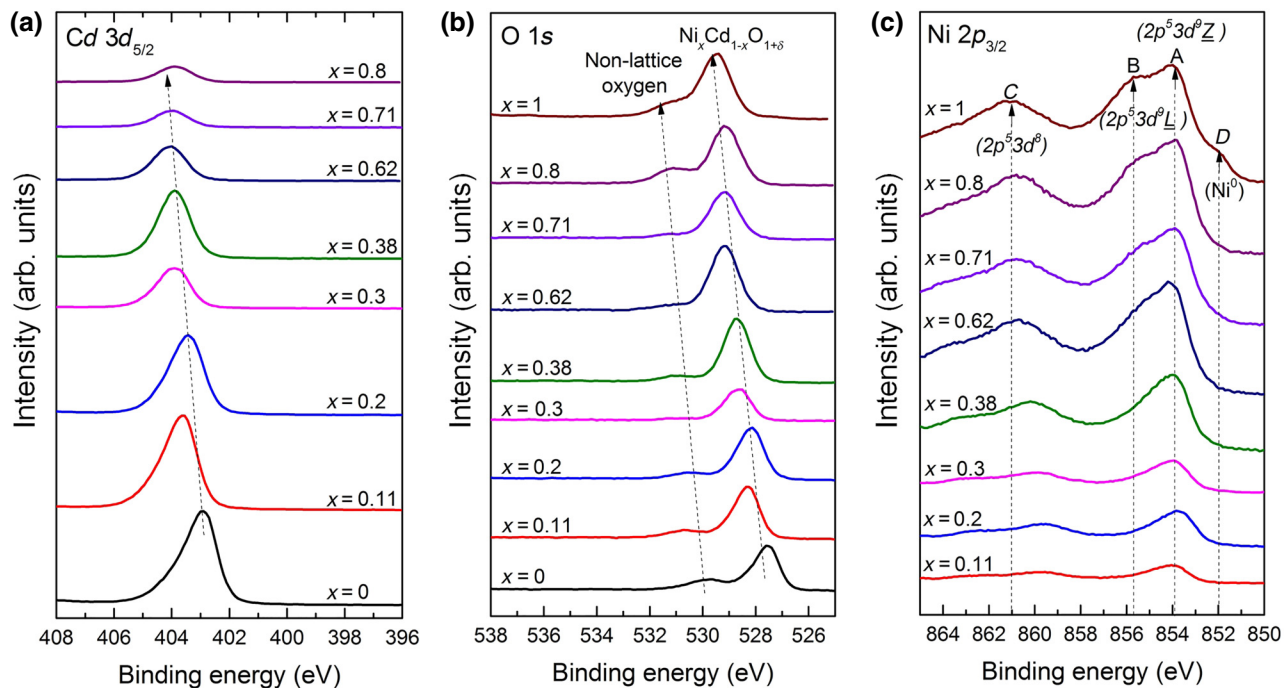

FIG. 6.   High-resolution XPS core-level spectra of Cd $3d_{5/2}$ (a), O $1s$ (b) and Ni $2p_{3/2}$ (c) for $Ni_xCd_{1-x}O_{1+\delta}$-alloy films with different Ni content x.

much faster reduction of the electron concentration than in stoichiometric alloys. This is clearly confirmed by the results in Fig. 3 where the electron concentration drops by five orders of magnitude as x increases to about 0.38. At $x > 0.38$, the donor concentration falls below the acceptor concentration and the alloy becomes p type with holes conducting in the E_{V1} subband. As seen in Fig. 5, in the intermediate composition range, the E_{V1} subband is highly localized, which explains extremely low hole mobilities for $0.38 < x < 0.6$. The noticeable enhancement of the hole mobility in the composition region of about $x = 0.8$ can be attributed to a wider, less-localized hole-conducting E_{V1} band.

The proposed picture of the electronic band structure can also help to understand the difference between the optical properties of stoichiometric and O-rich alloys. In stoichiometric $Ni_xCd_{1-x}O$ alloy, the E_{C2} subband is occupied and the only significant optical transitions occur between E_{V2} and E_{C1} subbands. The Ni d-levels affect these transitions only through the anticrossing interactions that push E_{C1} up and E_{V2} down close to the crossing compositions of about $x = 0.2$ and 0.7, respectively. As a result, the optical gap shows the unusual positive bowing parameter illustrated in Fig. 2(c) and discussed in Ref. [38]. The main difference between stoichiometric and O-rich alloys is that at $x = 0.38$, the nonstoichiometric alloy becomes p type with the Fermi energy shifting down to the E_{V1} valence subband. This allows for optical transitions from p-like symmetry E_{V2} to d-like symmetry E_{C2}. An absorption spectrum associated with these transitions will be significantly broadened because of the highly localized nature of the final E_{C2} subband states. Also, as is evident from Fig. 5, the absorption spectrum is expected to shift to lower energy with increasing Ni content. The results of optical absorption shown in Fig. 2(b) are in qualitative agreement with this interpretation.

In order to better understand the electronic properties of RT-deposited $Ni_xCd_{1-x}O_{1+\delta}$-alloy films, high-resolution core-level XPS spectra of the O $1s$, Cd $3d_{5/2}$, and Ni $2p_{3/2}$ regions are recorded for samples with different x. All spectra are recorded after a brief Ar^+ sputtering to remove the surface contamination. The binding energies are referenced to the C $1s$ (collected without Ar^+ sputtering) at 284.8 eV. As shown in Fig. 6(a), the Cd $3d_{5/2}$ core level peak shifts gradually from approximately 403 eV ($x = 0$) to approximately 404 eV ($x \sim 0.8$) as alloy composition x increases. The measured Cd $3d_{5/2}$ peak position for the pure CdO is comparable to values reported by others [35]. Figure 6(b) shows the O $1s$ core level spectra for selected $Ni_xCd_{1-x}O_{1+\delta}$-alloy films. Apparently, these O $1s$ spectra can be resolved into two components, a strong low-binding energy (E_b) component and a weak high-binding energy E_b component. The strong lower O $1s$ E_b gradually shifts from 527.6 eV ($x = 0$) to 529.5 eV ($x = 1$). The lower O $1s$ E_b for the two end-point materials (i.e., CdO and NiO)

are consistent with reported values [35,57]. The monotonic shift of this strong O $1s$ peak confirms that the RT-sputtered films are random alloys. On the other hand, the weak high-E_b component is likely due to the oxygen not in the lattice position (e.g., O interstitials, surface-adsorbed OH group, COOH, Ni_2O_3, etc.) within these alloy films [58]. For nonstoichiometric $NiO_{1+\delta}$, this high E_b (approximately 531 eV) O $1s$ peak has been frequently assigned to the Ni^{3+} related phase (e.g., Ni_2O_3) [59,60]. However, we should mention that the high E_b (approximately 531 eV) O $1s$ peak is also found in the NiO film sputtered in pure Ar (not shown). Hence, a quantitative correlation between this high-E_b peak with hole concentration cannot be established [61].

Fig. 6(c) shows Ni $2p_{3/2}$ spectra of $Ni_xCd_{1-x}O_{1+\delta}$-alloy films. The characteristic features of $Ni_xCd_{1-x}O_{1+\delta}$ at approximately 854, 855.8, and 861 eV are labeled as peaks A, B, and C, corresponding to the Zhang-Rice doublet bound states near the Fermi level and a hole in the O $2p$ ligand states, respectively [62,63]. The peak B in the Ni $2p_{3/2}$ spectrum of NiO has also been frequently attributed to the Ni^{3+} (e.g., Ni_2O_3) states or due to the superposition of a correlation effect and Ni^{3+} species localized close to the surface [62,64,65]. Notice that the intensity ratio of peaks B to A increases with increasing x. This may suggest an increase in the Ni^{3+} in the film. However, when we compare the Ni $2p$ spectra of NiO films sputtered in 0% and 1.4% O_2, we find no noticeable difference, implying that feature B is likely not related to the deviation of oxygen stoichiometry. The small metallic Ni (Ni^0, $E_b \sim 852$ eV) peak in Ni $2p_{3/2}$ spectra from an alloy film with $x > 0.95$ is most likely due to the Ar^+ sputtering process which reduces the NiO forming some metallic Ni clusters [66].

XPS VB spectra for $Ni_xCd_{1-x}O_{1+\delta}$-alloy films are shown in Fig. 7. The VB of CdO is mainly composed of O $2p$, Cd $4s$, and Cd $4d$ states [35], while the VB of NiO is dominated by the Ni $3d^8\underline{Z}$ and Ni $3d^8\underline{L}$ states [63], which are schematically shown at the bottom and top of Fig. 7, respectively. Here $\underline{Z}$ and $\underline{L}$ represent a hole in the bounding state and a hole in O $2p$ ligand state, respectively. We notice that the features of VB spectra of these $Ni_xCd_{1-x}O_{1+\delta}$ gradually change as the Ni content x varies. Using the same procedure as in reference [67], we assume that the Fermi level is pinned at the surface at the Fermi stabilization energy E_{FS} (-4.9 eV) and fitting the XPS spectra (Fig. 7) by convoluting a step function with a Gaussian function, the VBMs with respect to vacuum are plotted as square symbols in Fig. 5. For the NiO-rich alloys, the measured VBM agree qualitatively with the position of the highest lying valence subband E_{V1}. We note that the position of the VBM obtained from XPS VB spectra may have contributions from the bulk, and therefore, may not be pinned at E_{FS}. For Cd-rich alloys, the VBMs will be affected by the higher lying VBM of CdO at the L-point.
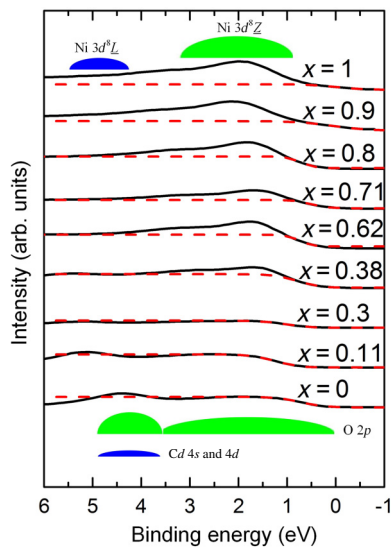
FIG. 7. XPS valence-band spectra of $Ni_xCd_{1-x}O_{1+\delta}$. The dashed line spectra are fits to the XPS spectra with a step function convoluted with a Gaussian function. The O $2p$ (denoted in green) and Cd $4s$ and $4d$ (denoted in blue) states of CdO are schematically shown at the bottom, while the Ni $3d^8\underline{Z}$ (green) and Ni $3d^8\underline{L}$ (blue) states of NiO are depicted at the top.

IV. CONCLUSIONS

Nanocrystalline NiO-CdO-alloy thin films over the entire composition range are synthesized by radio-frequency magnetron sputtering at RT. Alloys are sputter deposited in both pure Ar ($Ni_xCd_{1-x}O$) and Ar + O_2 ($Ni_xCd_{1-x}O_{1+\delta}$) environments. All of the alloy films are nanocrystalline in the rock salt structure. The $Ni_xCd_{1-x}O$-alloy films sputtered in Ar with $x < 0.52$ exhibit n-type conductivity and become insulating for films with higher x. When sputtered with 1.4% O_2, the $Ni_xCd_{1-x}O_{1+\delta}$-alloy films with $x \leq 0.3$ are n type with higher resistivity than $Ni_xCd_{1-x}O$ films, but they become p-type conducting when $x \geq 0.38$. Hence, we have identified NiO-CdO-alloy films within an alloy region of $0.38 \leq x \leq 0.52$ that exhibit both n- and p-type conductivity, depending on the growth conditions. Within this composition range, the band gap of the alloy is approximately 3–3.3 eV with transmittance >50% in the visible range. A p-n homojunction based on n $Ni_xCd_{1-x}O$ and p $Ni_xCd_{1-x}O_{1+\delta}$ in this composition can be expected. The unusual electrical and optical properties of $Ni_xCd_{1-x}O_{1+\delta}$-alloy thin films can be explained by the modifications of the electronic band structure due to anti-crossing interactions between localized Ni d levels and extended VB and CB states of the alloy. In addition, we studied the transport mechanism of p-type $Ni_xCd_{1-x}O_{1+\delta}$-alloy films and found that the hole mobility increases with temperature in the range of 400–450 K. This is consistent with hole transport via a SPH process with an activation

energy E_a of 0.174 eV ($x = 1$) to 0.331 eV ($x = 0.47$). Furthermore, the resistivity of n- and p-type $Ni_xCd_{1-x}O_{1+\delta}$ films can be controlled by adjusting the O_2 partial pressure in the sputtering gas. These results strongly suggest that the nanocrystalline $Ni_xCd_{1-x}O_{1+\delta}$-alloy system has great technological potential for applications in transparent optoelectronic devices.

[1] Z. Wang, P. K. Nayak, J. A. C. Frescas, and H. N. Alshareef, Recent developments in p-type oxide semiconductor materials and devices, Adv. Mater. **28**, 3831 (2016).

[2] S. Nandy, A. N. Banerjee, E. Fortunato, and R. Martins, A review on Cu_2O and Cu-based p-type semiconducting transparent oxide materials: Promising candidates for new generation oxide based electronics, Rev. Adv. Sci. Engin. **2**, 273 (2013).

[3] M. A. Haque, A. D. Sheihk, X. Guan, and T. Wu, Metal oxides as efficient charge transporters in perovskite solar cells, Adv. Energy Mater. **7**, 1602803 (2017).

[4] J. L. Lyons, A. Janotti, and C. G. Van de Walle, Effect of hole localization on limiting p-type conductivity in oxide and nitride semiconductors, J. Appl. Phys. **115**, 012014 (2014).

[5] B. A. D. Williamson, J. Buckeridge, J. Brown, S. Ansbro, R. G. Palgrave, and D. O. Scanlon, Engineering valence band dispersion for high mobility p-type semiconductors, Chem. Mater. **29**, 2402 (2016).

[6] K. Ellmer, Magnetron sputtering of transparent conductive zinc oxide: Relation between the sputtering parameters and the electronic properties, J. Phys. D: Appl. Phys. **33**, R17 (2000).

[7] O. Bierwagen, Indium oxide-a transparent, wide-band gap semiconductor for (opto)electronic applications, Semicond. Sci. Technol. **30**, 024001 (2015).

[8] A. Wang, J. R. Babcock, N. L. Edleman, A. W. Metz, M. A. Lane, R. Asahi, V. P. Dravid, C. R. Kannewurf, A. J. Freeman, and T. J. Marks, Indium-cadmium-oxide films having exceptional electrical conductivity and optical transparency: Clues for optimizing transparent conductors, PNAS **98**, 7113 (2001).

[9] J. E. N. Swallow, B. A. D. Williamson, T. J. Whittles, M. Birkett, T. J. Featherstone, N. Peng, A. Abbott, M. Farnworth, K. J. Cheetham, P. Warren, D. O. Scanlon, V. R. Dhanak, and T. D. Veal, Self-compensation in transparent conducting F-doped SnO_2, Adv. Funct. Mater. **28,** 1701900 (2018).

[10] H. Kawazoe, M. Yasukawa, H. Hyodo, M. Kurita, H. Yanagi, and H. Hosono, P-type electrical conduction in transparent thin films of $CuAlO_2$, Nature **389,** 939 (1997).

[11] H. Yanagi, S. Inoue, K. Ueda, H. Kawazoe, and H. Hosono, Electronic structure and optoelectronic properties of transparent p-type conducting $CuAlO_2$, J. Appl. Phys. **88,** 4159 (2000).

[12] J. B. Varley, A. Miglio, V. A. Ha, M. J. V. Setten, G. M. Rignanese, and G. Hautier, High-throughput design of non-oxide p-type transparent conducting materials: Data mining, search strategy, and identification of boron phosphide, Chem. Mater. **29,** 2568 (2017).

[13] T. Jun, J. Kim, M. Sasase, and H. Hosono, Material design of p-type transparent amorphous semiconductor, Cu-S-I, Adv. Mater. **30,** 1706573 (2018).

[14] K. H. L. Zhang, K. Xi, M. G. Blamire, and R. G. Egdell, P-type transparent conducting oxides, J. Phys.: Condens. Matter. **28,** 383002 (2016).

[15] T. S. Tripathi and M. Karppinen, Atomic layer deposition of p-type semiconducting thin films: A review, Adv. Mater. Interfaces **4,** 1700300 (2017).

[16] X. Nie, S. H. Wei, and S. B. Zhang, Bipolar Doping and Band-Gap Anomalies in Delafossite Transparent Conductive Oxides, Phys. Rev. Lett. **86,** 066405 (2017).

[17] H. Hosono, Y. Ogo, H. Yanagi, and T. Kamiya, Bipolar conduction in SnO thin films, Electrochem. Solid-State Lett. **14,** H13 (2011).

[18] T. Arai, S. Iimura, J. Kim, Y. Yoda, S. Ueda, and H. Hosono, Chemical design and example of transparent bipolar semiconductor, J. Am. Chem. Soc. **139,** 17175 (2017).

[19] H. Sato, T. Minami, S. Takata, and T. Yamada, Transparent conducting p-type NiO thin films prepared by magnetron sputtering, Thin Solid Films **236,** 27 (1993).

[20] M. L. Grilli, F. Menchini, T. Dikonimos, P. Nunziante, L. Pilloni, M. Yilmaz, A. Piegari, and A. Mittiga, Effect of growth parameters on the properties of RF-sputtered highly conductive and transparent p-type NiO_x films, Semicond. Sci. Technol. **31,** 055016 (2016).

[21] P. Lunkenheimer, A. Loidl, C. R. Ottermann, and K. Bange, Correlated barrier hopping in NiO films, Phys. Rev. B **44,** 5927 (1991).

[22] J. M. McKay and V. E. Henrich, Structure of Valence and Conduction Levels in NiO, Phys. Rev. Lett. **53,** 2343 (1984).

[23] T. Dutta, P. Gupta, A. Gupta, and J. Narayan, Effect of Li doping in NiO thin films on its transparent and conducting properties and its application in heteroepitaxial p-n junctions, J. Appl. Phys. **108,** 083715 (2010).

[24] Y. A. K. Reddy, A. S. Reddy, and P. S. Reddy, Substrate temperature dependent properties of Cu doped NiO films deposited by DC reactive magnetron sputtering, J. Mater. Sci. Technol. **29,** 647 (2013).

[25] W. L. Jang, Y. M. Lu, W. S. Hwang, T. L. Hsiung, and H. P. Wang, Point defects in sputtered NiO films, Appl. Phys. Lett. **94,** 062103 (2009).

[26] H. B. Wu and L. S. Wang, A study of nickel monoxide (NiO), nickel dioxide (ONiO), and $Ni(O_2)$ complex by anion photoelectron spectroscopy, J. Chem. Phys. **107,** 16 (1997).

[27] R. Deng, B. Yao, Y. F. Li, Y. M. Zhao, B. H. Li, C. X. Shan, Z. Z. Zhang, D. X. Zhao, J. Y. Zhang, D. Z. Shen, and X. W. Fan, X-ray photoelectron spectroscopy measurement of n-ZnO/p-NiO heterostructure valence-band offset, Appl. Phys. Lett. **94,** 022108 (2009).

[28] W. Nie, H. Tsai, J. C. Blancon, F. Liu, C. C. Stoumpos, B. Traore, M. Kepenekian, O. Durand, C. Katan, S. Tretiak, J. Crochet, P. M. Ajayan, M. G. Kanatzidis, J. Even, and A. D. Mohite, Critical role of interface and crystallinity on the performance and photostability of perovskite solar cell on nickel oxide, Adv. Mater. **30,** 1703879 (2018).

[29] X. B. Xu, Z. H. Liu, Z. X. Zuo, M. Zhang, Z. X. Zhao, Y. Shen, H. P. Zhou, Q. Chen, Y. Yang, and M. K. Wang, Hole selective NiO contact for efficient perovskite solar cells with carbon electrode, Nano Lett. **15,** 2402 (2015).

[30] S. Seo, I. Park, M. Kim, S. Lee, C. Bae, H. Jung, N.-G. Park, J. Kim, and H. Shin, An ultra-thin, un-doped NiO hole transporting layer of highly efficient (16.4%) organic-inorganic hybrid perovskite solar cells, Nanoscale **8,** 11403 (2016).

[31] M. Yan, M. Lane, C. R. Kannewurf, and R. P. H. Chang, Highly conductive epitaxial CdO thin films prepared by pulsed laser deposition, App. Phys. Lett. **78,** 2342 (2001).

[32] K. M. Yu, M. A. Mayer, D. T. Speaks, H. He, R. Zhao, L. Hsu, S. S. Mao, E. E. Haller, and W. Walukiewicz, Ideal transparent conductors for full spectrum photovoltaics, J. Appl. Phys. **111,** 123505 (2012).

[33] C. P. Liu, C. Y. Ho, C. K. Kwok, P. F. Guo, M. K. Hossain, J. A. Zapien, and K. M. Yu, High mobility transparent amorphous CdO-In_2O_3 alloy films synthesized at room temperature, Appl. Phys. Lett. **111,** 072108 (2017).

[34] L. F. J. Piper, L. Colakerol, P. D. C. King, A. Schleife, J. Zuniga-Perez, P. A. Glans, T. Learmonth, A. Federov, T. D. Veal, F. Fuchs, V. Munoz-Sanjose, F. Bechstedt, C. F. McConville, and K. E. Smith, Observation of quantized subband states and evidence for surface electron accumulation in CdO from angle-resolved photoemission spectroscopy, Phys. Rev. B **78,** 165127 (2008).

[35] P. D. C. King, T. D. Veal, A. Schleife, J. Z. Perez, B. Martel, P. H. Jefferson, F. Fuchs, V. M. Sanjose, F. Bechstedt, and C. F. McConville, Valence-band electronic structure of CdO, ZnO, and MgO from x-ray photoemission spectroscopy and quasi-particle-corrected density-functional theory calculations, Phys. Rev. B **79,** 205205 (2009).

[36] C. A. Francis, D. M. Detert, G. Chen, O. D. Dubon, K. M. Yu, and W. Walukiewicz, $Ni_xCd_{1-x}O$: Semiconducting alloys with extreme type III band offsets, Appl. Phys. Lett. **106,** 022110 (2015).

[37] D. T. Speaks, M. A. Mayer, K. M. Yu, S. S. Mao, E. E. Haller, and W. Walukiewicz, Fermi level stabilization energy in cadmium oxide, J. Appl. Phys. **107,** 113706 (2010).

[38] C. A. Francis, M. Jaquez, J. F. S-Royo, S. K. V. Farahani, C. F. McConville, J. Beeman, M. Ting, K. M. Yu, O.

D. Dubon, and W. Walukiewicz, Effects of Ni d-levels on the electronicband structure of Ni$_x$Cd$_{1-x}$O semiconducting alloys, J. Appl. Phys. **122,** 185703 (2017).

[39] R. Newman and R. M. Chrenko, Optical properties of nickel oxide, Phys. Rev. **114,** 1507 (1959).

[40] Mizuki Ono, Kohei Sasaki, Hiroki Nagai, Tomohiro Yamaguchi, Masataka Higashiwaki, Akito Kuramata, Shigenobu Yamakoshi, Mitsunobu Sato, Tohru Honda, and Takeyoshi Onuma, Relation between electrical and optical properties of p-Type NiO films, Phys. Stat. Sol. B **255,** 1700311 (2018).

[41] E. Burstein, Anomalous optical absorption limit in InSb, Phys. Rev. **93,** 632 (1954).

[42] S. C. Jain, J. M. McGregor, and D. J. Roulston, Band-gap narrowing in novel III-V semiconductor, J. Appl. Phys. **68,** 3747 (1990).

[43] Y. Zhu, R. J. Mendelsberg, J. Zhu, J. Han, and A. Anders, Structural, optical and electrical properties of indium-doped cadmium oxide films prepared by pulsed filtered cathodic arc deposition, J. Mater. Sci. **48,** 3789 (2013).

[44] V. P. Zhuze and A. I. Shelykh, Hall effect in nickel oxide, Soviet Phys.-Solid State **5,** 1278 (1963).

[45] H. J. V. Daal and A. J. Bosman, Hall effect in CoO, NiO, and α-Fe$_2$O$_3$, Phys. Rev. **158,** 736 (1967).

[46] T. Kamiya, K. Nomura, and H. Hosono, Present status of amorphous In-Ga-Zn-O thin-film transistors, Sci. Technol. Adv. Mater. **11,** 044305 (2010).

[47] R. Karsthof, P. Racke, H. von Wenckstern, and M. Grundmann, Semi-transparent NiO/ZnO UV photovoltaic cells, Phys. Status Aolidi A **213,** 30 (2016).

[48] W. Chen, Y. Wu, J. Fan, A. B. Djurisic, F. Liu, H. W. Tam, A. Ng, C. Surya, W. K. Chan, D. Wang, and Z. B. He, Perovskite solar cell: Understanding the doping effect on NiO: Toward high-performance inverted perovskite solar cells, Adv. Energy Mater. **8,** 1870091 (2018).

[49] G. Niu, S. Wang, J. Li, W. Li, and L. Wang, Oxygen doping in nickel oxide for highly efficient planar perovskite solar cells, J. Mater. Chem. A **6,** 4721 (2018).

[50] M. Grundmann, F. Klupfel, R. Karsthof, P. Schlupp, F. L. Schein, D. Splith, C. Yang, S. Bitter, and H. von Wenckstern, Oxide bipolar electronics: Materials, devices and circuits, J. Phys. D: Appl. Phys. **49,** 213001 (2016).

[51] A. Banerjee, S. Pal, and B. K. Chaudhuri, Nature of small-polaron hopping conduction and the effect of Cr doping on the transport properties of rare-earth manganite La$_{0.5}$Pb$_{0.5}$Mn$_{1-x}$Cr$_x$O$_3$, J. Chem. Phys. **115,** 1550 (2001).

[52] N. Mott, *Electronic Processes in Non-Crystalline Materials* (Clarendon, Oxford, 1971).

[53] G. J. Snyder, R. Hiskes, S. Dicarolis, M. R. Beasley, and T. H. Geballe, Intrinsic electrical transport and magnetic properties of La$_{0.67}$Ca$_{0.33}$MnO$_3$ and La$_{0.67}$Sr$_{0.33}$MnO$_3$ MOCVD thin films and bulk material, Phys. Rev. B **53,** 14434 (1996).

[54] Y. Nishi, T. Iwata, and T. Kimoto, Correlation between oxygen composition and electrical properties in NiO thin films for resistive random access memory, Jpn. J. Appl. Phys. **50,** 015802 (2011).

[55] J. Y. Zhang, W. W. Li, R. L. Z. Hoye, J. L. M. Driscoll, M. Budde, O. Bierwagen, L. Wang, Y. Du, M. J. Wahila, L. F. J. Piper, T. L. Lee, H. J. Edwards, V. R. Dhanak, and K. H. L. Zhang, Electronic and transport properties of Li-doped NiO epitaxial thin films, J. Mater. Chem. C **6,** 2275 (2018).

[56] W. Walukiewicz, Intrinsic limitations to the doping of wide-gap semiconductors, Physica B **302–303,** 123 (2001).

[57] M. C. Biesinger, B. P. Payne, L. W. M. Lau, A. Gerson, and R. St. C. Smart, X-ray photoelectron spectroscopic chemical state quantification of mixed nickel metal, oxide and hydroxide system, Surf. Interface Anal. **41,** 324 (2009).

[58] P. R. Norton, R. L. Tapping, and J. W. Goodale, A photoemission study of the interaction of Ni (100), (110) and (111) surfaces with oxygen, Surf. Sci. **65,** 13 (1977).

[59] S. Oswald and W. Bruckner, XPS depth profile analysis of non-stoichiometric NiO films, Surf. Interface Anal. **36,** 17 (2004).

[60] D. H. Kwon, S. R. Lee, Y. S. Choi, S. B. Son, K. H. Oh, K. Char, and M. Kim, Observation of the Ni$_2$O$_3$ phase in a NiO thin-film resistive switching system, Phys. Status Solidi RRL **11,** 1700048 (2017).

[61] S. Uhlenbrock, C. Scharfschwerdt, M. Neumann, G. Illing, and H. J. Freund, The influence of defects on the Ni 2p and O 1s XPS of NiO, J. Phys.: Condens. Matter **4,** 7973 (1992).

[62] Y. Chen, O. Sakata, R. Yamauchi, A. Yang, L. S. R. Kumara, C. Song, N. Palina, M. Taguchi, T. Ina, Y. Katsuya, H. Daimon, A. Matsuda, and M. Yoshimoto, Lattice distortion and electronic structure of magnesium-doped nickel oxide epitaxial thin films, Phys. Rev. B **95,** 245301 (2017).

[63] M. Taguchi, M. Matsunami, Y. Ishida, R. Eguchi, A. Chainani, Y. Takata, M. Yabashi, K. Tamasaku, Y. Nishino, T. Ishikawa, Y. Senba, H. Ohashi, and S. Shin, Revisiting the Valence-Band and Core-Level Photoemission Spectra of NiO, Phys. Rev. Lett. **100,** 206401 (2008).

[64] Y. S. Chen, J. F. Kang, B. Chen, B. Gao, L. F. Liu, X. Y. Liu, Y. Y. Wang, L. Wu, H. Y. Yu, J. Y. Wang, Q. Chen, and E. G. Wang, Microscopic mechanism for unipolar resistive switching behavior of nickel oxides, J. Phys. D: Appl. Phys. **45,** 065303 (2012).

[65] F. Jiang, W. C. H. Choy, X. Li, D. Zhang, and J. Cheng, Post-treatment-free solution-processed non-stoichiometric NiO$_x$ nanoparticles for efficient hole-transport layers of organic optoelectronic devices, Adv. Mater. **27,** 2930 (2015).

[66] A. R. G. Elipe, J. P. Holgado, R. Alvarez, and G. Munuerz, Use of factor analysis and XPS to study defective nickel oxide, J. Phys. Chem. **96,** 3080 (1992).

[67] C. P. Liu, C. Y. Ho, R. D. Reis, Y. Foo, P. F. Guo, J. A. Zapien, W. Walukiewicz, and K. M. Yu, Room-temperature-synthesized high-mobility transparent amorphous CdO-Ga$_2$O$_3$ alloys with widely tunable electronic bands, ACS Appl. Mater. Interfaces **10,** 7239 (2018).